C-Terminus Loop 13 of Na^+ Glucose Cotransporter SGLT1 Contains a Binding Site for Alkyl Glucosides†

M. Mobeen Raja, Helmut Kipp, and Rolf K. H. Kinne*

Department of Epithelial Cell Physiology, Max Planck Institute of Molecular Physiology, Otto-Hahn-Strasse 11, 44227 Dortmund, Germany

Received May 3, 2004; Revised Manuscript Received June 20, 2004

ABSTRACT: Recently, we identified the extramembranous C-terminus loop 13 of SGLT1 as a binding site for the aromatic glucoside phlorizin, which competitively inhibits sodium D-glucose cotransport. Alkyl glucosides are also competitive inhibitors of the transport. Therefore, in this study, we searched for potential binding sites for alkyl glucosides in loop 13. To this end, we synthesized a photoaffinity label (2′-Azi-*n*-octyl)-*β*-D-glucoside and analyzed the region of attachment using MALDI mass spectrometry, producing wild-type recombinant truncated loop 13. Furthermore, we prepared four single-Trp mutants of the loop and determined their fluorescence, its change in the presence of alkyl glucosides, and their accessibility to acrylamide. Photolabeling of truncated loop 13 with (2′-Azi-*n*-octyl)-*β*-D-glucoside revealed an attachment of the C2 group of the alkyl chain to Gly-Phe-Phe-Arg (amino acid residues 598−601). In the presence of *n*-hexyl-*β*-D-glucoside, all mutants (R601W, D611W, E621W, and L630W) exhibited a significant decrease in Trp fluorescence with an apparent binding affinity of 8−14 *μ*M. Only L630W exhibited a significant blue shift, and only in R601W was a change in acrylamide quenching (protection) observed. No quenching or protection was found for D-glucose; however, 1-hexanol produced the same results as *n*-hexyl-*β*-D-glucoside. The interaction shows stereoselectivity for *n*-hexyl-*β*-D-glucoside binding; the *β*-configuration of the sugar moiety at C1, the *cis* conformation of the unsaturated alkenyl side chain in the C3−C4 bond, and the alkyl chain length of six to eight carbon atoms lead to an optimum interaction. A schematic two-dimensional model was derived in which C2 interacts with the region around residue 601, C3 and C4 interact with the region between residues 614 and 619, and C6−C8 interact with the region between residues 621 and 630. The data demonstrate that loop 13 provides binding sites for alkyl glucosides as well as for phlorizin; thus, loop 13 of SGLT1 seems to be a major binding domain for the aglucone residues of competitive D-glucose transport inhibitors.

Ion-coupled cotransport systems are critically involved in the absorption and secretion of inorganic and organic solutes across epithelia (*1*−*3*). Na^+ D-glucose cotransporters (SGLTs) play a major role in D-glucose absorption by utilizing the inwardly directed Na^+ ion gradient as a driving force for the accumulation of sugars across the brush border membrane of kidney proximal tubules and the small intestine. Recently, SGLT1[1] has been identified as a potential target in the treatment of diabetes, and inhibitors of the transporter are therefore of renewed interest (*4*, *5*). The cotransport system is inhibited by glucosides with either aromatic or aliphatic aglucone residues. Recently, we showed that phlorizin, an aromatic glucoside, binds to recombinant loop 13 of SGLT1 via the aromatic aglucone moiety, inducing conformational changes in the loop (*6*, *7*) predominantly in the region of amino acids 600−611.

Alkyl glucosides, also, have been demonstrated to inhibit sodium D-glucose cotransport in brush border membrane vesicles (*8*, *9*). In the study presented here, we therefore asked whether alkyl glucosides also bind to loop 13 of SGLT1 and, if so, whether they interact with the same amino acids. For this purpose, we expressed and purified the truncated loop 13 and performed photoaffinity labeling with a newly synthesized diazirino analogue of octyl glucoside, (2′-Azi-*n*-octyl)-*β*-D-glucoside, *in vitro*. Furthermore, we conducted fluorescence measurements of loop 13 mutants in which Trp residues were placed at different positions of the loop as reporter groups.

In the photoaffinity labeling experiments, a binding of C2 of the alkyl chain to the area between amino acids 598 and 601 of loop 13 was identified. The fluorescence signals confirmed this binding region and revealed further interactions in the area between amino acids 614 and 619 and at amino acid 630. Thus, loop 13 also provides, indeed, a binding region for alkyl glucoside; the areas of interaction and the conformational changes induced differ, however, significantly from those found for phlorizin. This opens new

† This work was supported by funds of the IMPRS-CB (International Max Planck Research School in Chemical Biology).

* To whom correspondence should be addressed: Department of Epithelial Cell Physiology, Max Planck Institute of Molecular Physiology, Otto-Hahn-Str. 11, 44227 Dortmund, Germany. E-mail: rolf.kinne@mpi-dortmund.mpg.de. Telephone: +49 (0) 231−133 2200. Fax: +49 (0) 231−133 2299.

[1] Abbreviations: SGLT1, Na^+ glucose cotransporter; SDS−PAGE, sodium dodecyl sulfate−polyacrylamide gel electrophoresis; PBS, phosphate-buffered saline; Bis-Tris, 2-[bis(2-hydroxyethyl)amino]-2-(hydroxymethyl)propane-1,3-diol; MALDI-TOF, matrix-assisted laser desorption ionization time-of-flight; BBMV, brush border membrane vesicles; EA, ethyl acetate; ME, methanol; PE, low-boiling point petroleum ether (40−60 °C); W, water.

10.1021/bi049106n CCC: $27.50
Published on Web 08/07/2004

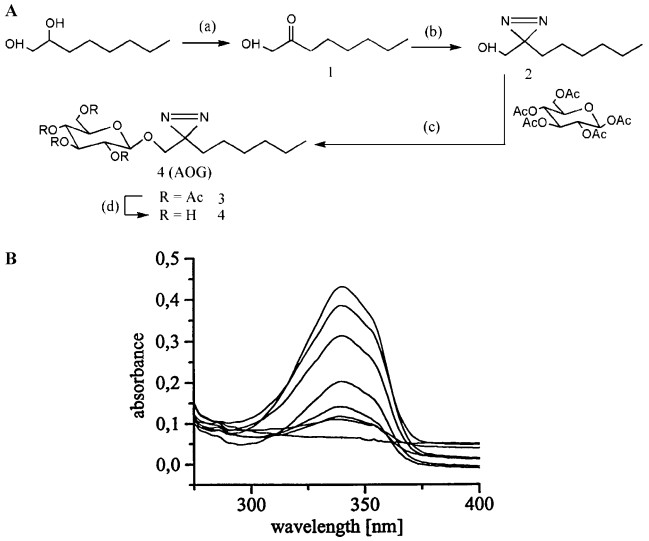

FIGURE 1: (A) Synthesis of (2′-Azi-*n*-octyl)-*β*-D-glucoside (AOG) **4**. The reagents were (a) NaOCl, (b) NH_3, I_2, triethylamine, and hydroxylamine-*O*-sulfonic acid, (c) *β*-D-glucoside pentaacetate and $SnCl_4$, and (d) NaOMe. (B) UV spectra of a solution of (2′-Azi-*n*-octyl)-*β*-D-glucoside (5.5 mM) in phosphate buffer [50 mM KH_2PO_4-KOH (pH 7.4)] irradiated for different periods of time (0, 0.5, 1, 2, 3, 4, 5, and 30 min). The half-life of the decomposition was estimated from a logarithmic plot of the absorbance data vs the irradiation time ($\tau_{1/2} = 1.5$ min, $\lambda_{max} = 340$ nm, and $\epsilon = 53$ M^{-1} cm^{-1}).

possibilities for a model-guided synthesis of glucose transport inhibitors.

EXPERIMENTAL PROCEDURES

Materials. Chemicals used in synthesis were reagent grade and purchased from either Fluka (Neu-Ulm, Germany) or Aldrich (Steinheim, Germany), including EDTA, Tris base, glycine, NaCl, L-Trp, phlorizin, *n*-hexyl-*β*-D-glucoside, *trans*-*n*-3-hexenyl-*β*-D-glucoside, *cis*-*n*-3-hexenyl-*β*-D-glucoside, *n*-octyl-*β*-D-glucoside, *n*-decyl-*β*-D-glucoside, 1-hexanol, isopropyl-*β*-D-thiogalactopyranoside, and 2,5-dihydroxybenzoic acid.

Chemical Synthesis. The chemical synthesis of (2′-Azi-*n*-octyl)-*β*-D-glucoside (**4**) is shown in Figure 1. *n*-Octanol-1,2-diol was used as the starting material. Instrumentation and abbreviations were used as described previously (*9*).

*2-Oxo-n-octanol-1 (**1**).* *n*-Octanol-1,2-diol (10.0 g, 68.4 mmol) was used as a starting material and dissolved in 50 mL of acetic acid. A solution of sodium hypochlorite (60 mL, 13%, 118 mmol) was added dropwise at room temperature over a period of 30 min to a stirred solution of *n*-octanol-1,2-diol. The reaction mixture was further stirred for 3 h at room temperature, diluted with 200 mL of water, and extracted three times with 75 mL of dichloromethane. The organic phase was separated and neutralized three times with 100 mL of a saturated solution of sodium hydrogen carbonate. The combined dichloromethane extracts were washed with 100 mL of water, dried with $MgSO_4$, and evaporated *in vacuo* to yield 7.95 g (81%) of **1** as a syrup: TLC (EA-PE, 1:1) $R_f = 0.48$; IR υ_{max} (film) 1700 (C═O), 3400 cm^{-1} (OH); ^{1}H NMR ($CDCl_3$, 500 MHz) δ 0.89 (t, 3H, H-8), 1.29 (m, 6H), 1.63 (m, 2H), 2.41 (t, 2H, H-3), 3.26 (s, 1H, OH), 4.24 (s, 2H, H-1); ^{13}C NMR ($CDCl_3$, 125.8 MHz) δ 14.01, 22.49, 23.73, 28.91, 31.52, 38.46 (C-3−C-8), 68.13 (C−OH), 210.03 (C═O).

*2-Azi-n-octanol-1 (**2**).* A stream of dry NH_3 was introduced into a solution of 2.84 g (19.7 mmol) of **1** in 150 mL of dry ME at −30 °C until the volume of the reaction mixture increased ∼20%. Then, 3.8 g (33.7 mmol) of hydroxylamine-*O*-sulfonic acid was added in small portions over a period of 1 h to the vigorously stirred mixture. The suspension was stirred for 3 h at −30 °C, allowed to warm to room temperature and held there for 18 h, filtered, and concentrated *in vacuo*. A solution of the residue in 100 mL of dry ME containing 20 mL of triethylamine was cooled to 0 °C, and iodine was added until the red color persisted. The solution was then concentrated, and the syrup was dissolved in 100 mL of dichloromethane. The organic phase was separated two times with 50 mL of a sodium thiosulfate solution (5%) with vigorous shaking. The combined organic extracts were washed two times with 50 mL of water, dried with $MgSO_4$, evaporated *in vacuo*, and purified by column chromatography (5 cm × 17 cm, EA-PE, 1:3) to give 2.08 g (68%) of crude **2**: TLC (EA-PE, 1:1) $R_f = 0.56$, λ_{max} (ME) = 344 nm (log $\epsilon = 1.81$); IR υ_{max} (film) 3350 cm^{-1} (OH; no C═O); ^{1}H NMR ($CDCl_3$, 500 MHz) δ 0.87 (t, 3H, H-8), 1.13 (m, 2H), 1.27 (m, 6H), 1.45 (t, 2H, H-3), 2.15 (s, 1H, OH), 3.49 (s, 2H, H-1); ^{13}C NMR ($CDCl_3$, 125.8 MHz) δ 14.01, 22.51, 23.40, 23.55, 28.89, 29.70, 31.58 (C-2−C-8), 63.93 (C−OH).

*(2′-Azi-n-octanol)-2,3,4,6-tetra-O-acetyl-β-D-glucopyranoside (**3**).* The compounds 2-Azi-*n*-octanol (**2**) (0.78 g, 5 mmol) and 1,2,3,4,6-penta-*O*-acetyl-*β*-D-glucopyranoside (2.93 g, 7.5 mmol) were dissolved in 150 mL of dry dichloromethane in the presence of 2.0 g of molecular sieves (4 Å) for 30 min at room temperature. Then tin(IV) chloride was added, and the reaction mixture was allowed to stir at room temperature for 5 h. The reaction mixture was neutralized dropwise with saturated aqueous $NaHCO_3$. The organic phase was separated, extracted two times with 100 mL of dichlorometane, washed with water, dried with $MgSO_4$, and concentrated *in vacuo*. The residue was purified on a silica column [5 cm × 17 cm, EA-PE, 1:1, $R_f = 0.52$, λ_{max} (ME) = 339 nm (log $\epsilon = 1.81$)]: ^{1}H NMR ($CDCl_3$, 500 MHz) δ 0.87 (t, 3H, H-8), 1.10, 1.25, 1.43 (m, 10H, H-3′−H-7′), 2.01, 2.03, 2.08, (4 × s, 12H, 4 × H−Ac), 3.31 (d, 1H, H-1′a), 3.65 (d, 1H, H-1′b), 3.70 (m, 1H, H-5), 4.12 (dd, 1H, H-6a), 4.24 (dd, 1H, H-6b), 4.48 (d, 1H, H-1, $J_{1,2} = 7.9$ Hz), 4.98 (t, 1H, H-4), 5.08 (t, 1H, H-2, $J_{2,3} = 9.8$ Hz), 5.21 (t, 1H, H-3, $J_{3,4} = 9.4$ Hz); ^{13}C NMR ($CDCl_3$, 125.8 MHz) δ 14.15, 22.49, 23.40, 27.65, 28.83, 29.98, 31.53 (C-2′−C-8), 20.75 (4 × C−Ac), 61.80 (C-6), 68.31 (C-1′), 70.45, 71.10, 71.98, 72.68 (C-2−C-5), 100.13 (C-1), 169.29, 169.38, 170.28, 170.64 (4 × C−Ac).

*(2′-Azi-n-octanol)-β-D-glucopyranoside (**4**).* Compound tetra-*O*-acetate (**3**) (390 mg, 0.8 mmol) was deacetylated by stirring it with 10 mL of a NaOMe solution (0.01 M in dry ME) for 1 h at room temperature. The solution was neutralized with ion-exchange resin (Amberlite IR 100, H^+); the solvent was evaporated *in vacuo*, and the residue was purified on a silica column (3 cm × 17 cm, EA-ME-W, 27:2:1) to yield 230 mg (90%) of **4**: EA-ME, 4:1, $R_f = 0.49$, λ_{max} (ME) = 341 nm (log $\epsilon = 1.77$).

Renal BBMV and Transport Measurements. BBMV from hog kidney cortex were prepared by the magnesium precipitation method (*10*). Final BBMV were suspended at a concentration of 20 mg/mL protein in MHT buffer [100 mM

mannitol and 20 mM Hepes-Tris (pH 7.4)] and stored at −70 °C until use. The transport studies were carried out as described previously (*8*).

Preparation of Recombinant Peptides. Mutagenesis experiments were performed using the Chameleon Double Stranded, Site-directed Mutagenesis Kit (Stratagene, CA) as described previously (*6*). The mutations were the same as those used for the previous phlorizin binding studies (*6*) and included D611W, which showed the most prominent response (red shift, quenching, and increase in the accessibility of acrylamide) to the addition of phlorizin. The recombinant plasmids were transformed into BL21(DE3) cells for expression of 75-amino acid peptides of the wild type and Trp mutants of the C-terminus of SGLT1.

Peptide Expression and Purification. Amino-terminal GST tag peptides of the wild type and all mutants were expressed using 1 mM isopropyl-*β*-D-thiogalactopyranoside induction for 3.5 h at 37 °C in a 2 L culture. Cells were pelleted by centrifugation at 8000*g* for 10 min at 4 °C and resuspended in 20 mL of PBS lysis buffer [140 mM NaCl, 2.7 mM KCl, 10 mM Na_2HPO_4, and 1.8 mM KH_2PO_4 (adjusted to pH 7.3)] supplemented with 5 mM DTT, 0.1% Triton X-100, 1 mg/mL lysozyme, and Protease Inhibitor Cocktail (one tablet). Cells were effectively lysed using a SONOPULS Ultrasonic Homogenisation system under mild conditions. The lysate was centrifuged at 17000*g* for 45 min at 4 °C. The supernatants containing GST tag peptides were applied to glutathione−Sepharose columns (Amersham Biosciences, Freiburg, Germany) after being passed through a 0.2 *μ*m filter. Soluble fractions of truncated wild-type loop 13 and all mutants (amino acid residues 564−638) after removal of the protease inhibitor were generated by treating the glutathione−Sepharose-immobilized fusion peptide, derived from pGEX-4T-1, with 2 units of thrombin/mL of the column in PBS for 16 h at 4 °C. The purity of all peptides was assessed by SDS−PAGE using a precast Bis-Tris 4−12% gel in Tris-glycine running buffer and staining with Coomassie Blue. The purity of the peptides was at least 90%. All peptide concentrations were determined by the method of Lowry using bovine serum albumin as a standard (*11*).

Photoaffinity Labeling of Truncated Loop 13 with (2′-Azi-n-octyl)-β-D-glucoside. Photoaffinity labeling was performed with the photolabile alkyl glucoside analogue (2′-Azi-*n*-octyl)-*β*-D-glucoside, as previously reported (*12*, *13*). The photolabeling experiments were carried out in 100 *μ*L of PBS buffer (pH 7.3) containing 225 *μ*g of wild-type truncated loop 13 peptide and 1 mM (2′-Azi-*n*-octyl)-*β*-D-glucoside. The mixture was preincubated at room temperature in the dark for 5 min. After incubation, photolysis was carried out in a Rayonet RPR-100 photochemical reactor (Southern New England Ultraviolet Co., Branford, CT), and mass spectra were acquired in the positive ion, linear mode on a Voyager DE-PRO MALDI system (PE-Biosystems) as described previously (*6*).

Steady State Trp Fluorescence. The fluorescence experiments were performed at room temperature using a Perkin-Elmer LS 50B fluorescence spectrometer (Perkin-Elmer), following the same protocol described previously (*6*). All data were corrected for changes in fluorescence intensity by absorption or internal quenching.

Ligand Binding Assay. Fluorescence quenching was observed in the presence of various concentrations of *n*-hexyl-*β*-D-glucoside for each mutant. This signal was utilized to calculate the dissociation constants. Increasing amounts of *n*-hexyl-*β*-D-glucoside (from 1 to 350 *μ*M) were added to all mutants (5 *μ*M) in PBS. The corrected relative fluorescence intensity at different ligand concentrations was determined. Apparent binding constants were calculated using a single-site binding equation in the nonlinear regression analysis program Prism (Graphpad, San Diego, CA).

Quenching of Trp Fluorescence by Acrylamide. Trp fluorescence quenching experiments were performed in PBS (pH 7.3) for all mutants (5 *μ*M) in the presence and absence of 30 *μ*M *n*-hexyl-*β*-D-glucoside, *trans*-*n*-3-hexenyl-*β*-D-glucoside, *cis*-*n*-3-hexenyl-*β*-D-glucoside, *n*-octyl-*β*-D-glucoside, *n*-decyl-*β*-D-glucoside, or 1-hexanol. Acrylamide was added at room temperature as aliquots from a 5 M stock solution to each mutant peptide solution up to a final concentration of 350 mM. The accessibility of each Trp was monitored by analyzing the quenching data using a Stern−Volmer equation as described previously (*6*). The inner filter effects of the ligands found for the titration of a L-Trp solution (5 *μ*M) at an excitation of 295 nm and emission at 355 nm were found to be very weak; hence, they are not considered further in our measurements.

RESULTS

Synthesis and Properties of (2′-Azi-n-octyl)-β-D-glucoside. The synthesis of (2′-Azi-*n*-octyl)-*β*-D-glucoside is depicted in Figure 1. The secondary C2 hydroxy group of *n*-octanol-1,2-diol was converted into the corresponding carbonyl group via oxidation in the presence of NaOCl. The less reactive C2 carbonyl group of **1** could be easily converted into the diazirine group with the NH_3, hydroxylamine-*O*-sulfonic acid reagent and subsequent oxidation of the intermediate diaziridine with iodine (*20*, *21*). The selective glycosylation of 2-Azi-*n*-octanol-1 with C1 of *β*-D-glucose pentaacetate using $SnCl_4$ as a Lewis-acid catalyst gave compound **3**. (2′-Azi-*n*-octyl)-*β*-D-glucoside **4** was obtained after deacetylation of compound **3**.

The absorption maximum (Figure 1B) of the diazirine group of (2′-Azi-*n*-octyl)-*β*-D-glucoside is at 340 nm (ϵ = 53 M^{-1} cm^{-1}). On irradiation with long-wavelength UV lamp (λ_{max} = 350 nm) in a Rayonet photochemical reactor, (2′-Azi-*n*-octyl)-*β*-D-glucoside decomposes with a half-life of 1.5 min.

Interaction of (2′-Azi-n-octyl)-β-D-glucoside with the Sodium D-Glucose Cotransporter. To test whether the photoactive compound still interacted with SGLT1, its inhibitory action on sodium-dependent uptake of D-glucose into hog renal BBMV was investigated. As shown in Figure 2, (2′-Azi-*n*-octyl)-*β*-D-glucoside exhibits competitive inhibition characteristics with respect to D-glucose with a K_i of 43 ± 12 *μ*M. Compared to the inhibitory effect of *n*-octyl-*β*-D-glucoside (K_i = 30 ± 10 *μ*M) described previously (*9*), the modification of the molecule with the photolabile diazirine group at position C2 of the alkyl side chain did not significantly alter its affinity for the transporter.

Photolabeling of Truncated Loop 13 with (2′-Azi-n-octyl)-β-D-glucoside. To analyze directly whether alkyl glucosides interact with loop 13, photolabeling experiments with (2′-Azi-*n*-octyl)-*β*-D-glucoside were performed and analyzed by MALDI mass spectrometry. Figure 3A shows the expected

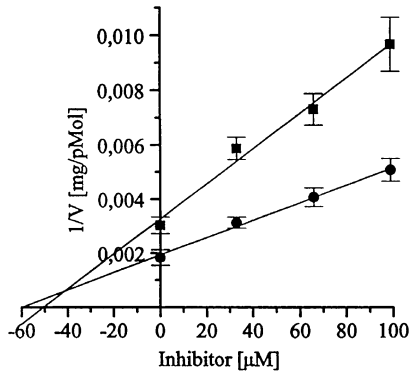

FIGURE 2: Inhibitory effects of (2′-Azi-*n*-octyl)-*β*-D-glucoside on D-glucose transport. Inhibitory effects of various concentrations of (2′-Azi-*n*-octyl)-*β*-D-glucoside on 5 s D-glucose uptake into hog kidney cortex BBMV measured at two substrate concentrations, 0.1 (■) and 0.2 mM (●) D-glucose, according to the method of Dixon. Results from representative experiments are shown. From three independent experiments, a K_i value of 43 ± 12 μM for (2′-Azi-*n*-octyl)-*β*-D-glucoside was calculated.

mass peak for loop 13 at *m*/*z* 8689.56 when no (2′-Azi-*n*-octyl)-*β*-D-glucoside was present. After photoaffinity labeling, an additional peak of *m*/*z* 9025.28 was observed (Figure 3B). The mass difference between the first peak (loop 13) and the second peak (*) corresponds to the mass of the photolyzed (2′-Azi-*n*-octyl)-*β*-D-glucoside. Another peak close to *m*/*z* 7700 was observed which probably represents a degradation product of the peptide. Furthermore, to determine the sites of interaction, photolabeled truncated loop 13 was digested in gel with trypsin. After extraction of the peptides from the gel, the resulting mixture was analyzed by MALDI-TOF. The only additional peak observed in the labeled probe was at *m*/*z* 845.05 (Figure 4A,B). This corresponds to an adduct of the Gly-Phe-Phe-Arg peptide of *m*/*z* 526.27 (amino acid residues 598−601) with the photolyzed (2′-Azi-*n*-octyl)-*β*-D-glucoside (*m*/*z* 318.78).

Effect of n-Hexyl-β-D-glucoside on the Fluorescence of Trp Mutants. We first tested whether *n*-hexyl-*β*-D-glucoside changed the steady state fluorescence of loop 13 mutants. The corrected Trp fluorescence spectra of R601W, D611W, E621W, and L630W in the presence and absence of *n*-hexyl-*β*-D-glucoside are shown in Figure 5A−D, respectively. Fluorescence quenching and shifts in the maximum were observed for each mutant, although to different extents. The fluorescence of R601W was quenched by 26% with a blue shift of 1 nm and that of D611W by 40% with a blue shift of ∼2 nm. Fluorescence quenching of ∼54% was found for E621W, and a slight red shift of 0.5−1 nm was observed. A fluorescence quenching of 46% with a remarkable blue shift of 3 nm was noted for L630W. The differences between the fluorescence quenching spectra of the various mutants, in particular, the shifts in the maxima, suggest that the various segments of loop 13 react differently to the binding of *n*-hexyl-*β*-D-glucoside.

Binding of n-Hexyl-β-D-glucoside to Single-Trp Mutants. The affinity of the mutants for *n*-hexyl-*β*-D-glucoside was determined by titration of the Trp mutants with different concentrations of *n*-hexyl glucoside, as shown in Figure 6. A maximum quenching of ∼55% of the fluorescence was observed for all mutants at high concentrations of *n*-hexyl-*β*-D-glucoside. The estimated equilibrium dissociation constants for all mutants are presented in Table 1. They are

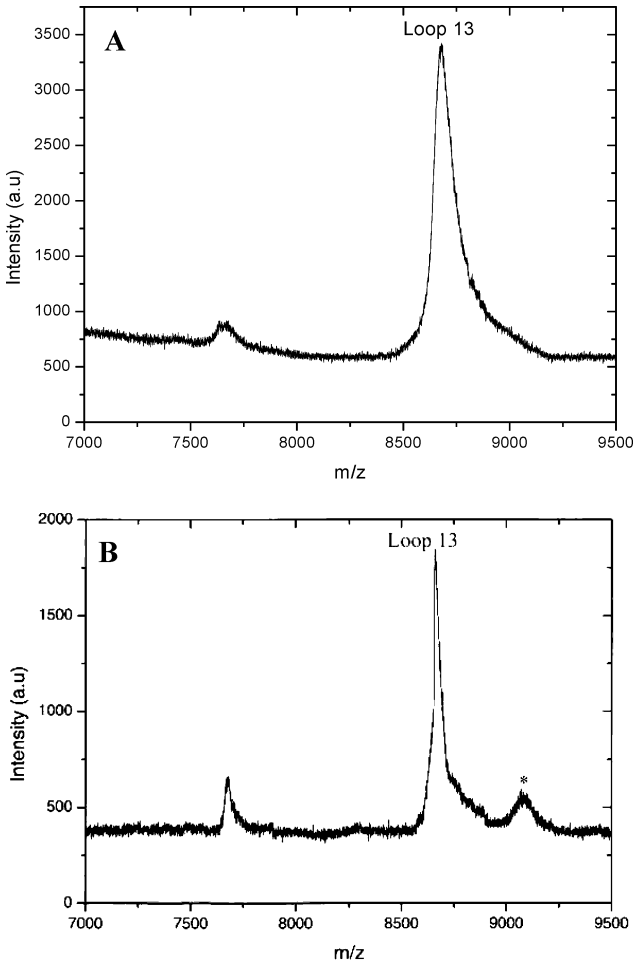

FIGURE 3: MALDI mass spectrometry of photoaffinity-labeled truncated loop 13. The peptide was incubated with (2′-Azi-*n*-octyl)-*β*-D-glucoside in PBS for 5 min in the dark at room temperature, followed by irradiation at 280 nm for 5 min. After being separated from noncovalently bound (2′-Azi-*n*-octyl)-*β*-D-glucoside by chloroform/methanol extraction, the peptide was dissolved in a 2,5-dihydroxybenzoic acid matrix: (A) truncated loop 13 (*m*/*z* 8689.56) before photoaffinity labeling and (B) truncated loop 13 after photoaffinity labeling. The asterisk denotes truncated loop 13 cross-linked with photolyzed (2′-Azi-*n*-octyl)-*β*-D-glucoside (*m*/*z* 9025.28). au, arbitrary units.

similar for all mutants and range from 8 to 14 μM, values comparable to the affinity of *n*-hexyl-*β*-D-glucoside for the intact SGLT1 in natural membranes (*9*).

Effect of n-Hexyl-β-D-glucoside on Trp Accessibility Monitored by Titration with Acrylamide. The water soluble collisional quencher acrylamide was used to measure the changes in accessibility of each Trp upon addition of *n*-hexyl-*β*-D-glucoside. The Stern−Volmer quenching plots in which F_0/F is plotted against the acrylamide concentration in the presence and absence of 30 μM *n*-hexyl-*β*-D-glucoside are shown in Figure 7A−D. All plots were linear with a regression coefficient of >0.99. The Stern−Volmer constants for all mutants are compiled in Table 1. Maximum protection was noted for mutant R601W, and slight protection was observed for D611W and L630W. In contrast, a slight increase in Trp accessibility was found for E621W.

Stereoselectivity of the Interaction of Alkyl Glucosides with Truncated Loop 13. In intact brush border membranes, a distinct stereoselectivity was observed for the interaction of alkyl glucosides with SGLT1 (*8*). The position of the residue at C1 (*β* vs α) or at the C3−C4 bond (*cis* vs *trans*) and the

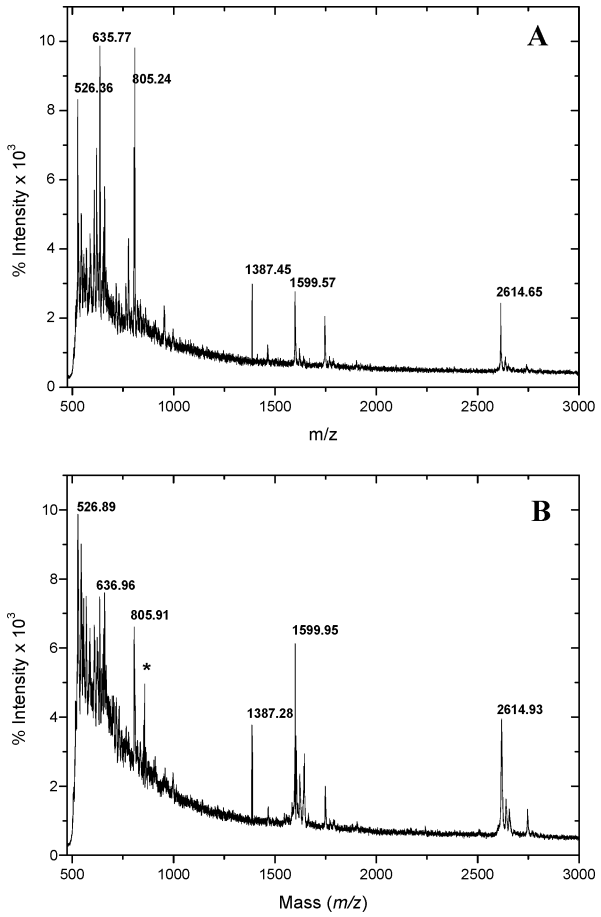

FIGURE 4: MALDI mass spectrum of photoaffinity-labeled truncated loop 13 after in-gel trypsin digestion. The truncated loop 13 was photolabeled with (2′-Azi-*n*-octyl)-*β*-D-glucoside; peptides were separated by SDS−PAGE, and peptide bands of interest were excised, destained, and digested in gel with trypsin. The peptides were extracted as described previously (*6*), and MALDI mass spectra were recorded: (A) Truncated loop 13 before photoaffinity labeling and (B) truncated loop 13 after photoaffinity labeling with (2′-Azi-*n*-octyl)-*β*-D-glucoside. The asterisk denotes the additional peak as an adduct to *m*/*z* 526.27 due to modification of the Gly-Phe-Phe-Arg peptide (amino acid residues 598−601) with photolyzed (2′-Azi-*n*-octyl)-*β*-D-glucoside (*m*/*z* 318.78).

chain length (C6−C10) turned out to be important. We therefore investigated the interaction of the corresponding compounds with loop 13 *in vitro*. As in the studies on intact membranes, the *β*-glucosides exhibited a more marked change in fluorescence than the α-glucosides, and the same holds for the preference of the *cis* versus the *trans* configuration at the C3−C4 bond. Extension of the alkyl chain beyond C6, however, reduced rather than increased the responses (see Table 2).

Effect of 1-Hexanol and D-Glucose on Trp Fluorescence and Accessibility to Acrylamide. To investigate which part of the alkyl glucoside, the sugar or the aglucone, is involved in the interaction with loop 13, 1-hexanol and D-glucose were used as ligands. The fluorescence of R601W was quenched upon addition of 100 *μ*M 1-hexanol by 45% with a red shift in maximum of 0.5−1 nm. Also, a significant protection effect was observed for 1-hexanol ($K_{SV} = 13\ M^{-1}$; also see Table 2 for comparison with the effect of *n*-hexyl-*β*-D-glucoside). D-Glucose (100 *μ*M) had no effect on either the fluorescence of R601W or the accessibility of Trp to acrylamide.

DISCUSSION

We observed basically three different parameters for the Trp fluorescence when *n*-hexyl-*β*-D-glucoside interacted with loop 13: (I) spectral shift in the fluorescence maximum, (II) fluorescence quenching, and (III) protection against acrylamide. Since the affinity of *n*-hexyl-*β*-D-glucoside for the different truncated loop 13 mutants is quite similar, the differences in parameters I and III are interpreted as an indication of different conformational changes in different portions of loop 13. A shift in maximum is considered to indicate a change in the hydrophobicity of the environment of the Trp under investigation, a blue shift points to increased and a red shift to decreased hydrophobicity. Such interpretation has been substantiated in various studies (*15*). The quenching we notice in this study is probably due to positioning of the Trp molecule in the proximity of methionine, tyrosine, threonine, arginine, and/or lysine (*16*, *17*) since the ligand *n*-hexyl-*β*-D-glucoside is spectroscopically silent. The protection against acrylamide is interpreted as a reduced accessibility of Trp caused by the fact that either the alkyl glucosides or a part of the loop shields Trp against the collision with acrylamide.

Using this interpretation, the changes in the fluorescence of the various regions can be explained by the following events. For Q581W and E591W mutants (data not shown), we did not observe any changes indicating that these positions do not participate in the interaction between loop 13 and *n*-hexyl-*β*-D-glucoside. In a way, this is to be expected since computer modeling suggests a random orientation of this part of loop 13.

The changes discussed below are compiled in the schematic model presented in Figure 8. For R601W, we observe a small blue shift of the maximum, a minor quenching, but maximum protection against acrylamide. The protection is probably caused by a strong binding of part of the alkyl glucoside in this area as also found in the photoaffinity labeling experiments where a direct interaction of the C2 position of the alkyl side chain with amino acids 598−601 could be demonstrated. The slight blue shift supports this assumption. These data furthermore suggest that the alkyl side chain is the part of the glucoside, which is binding. The experiments with 1-hexanol, where identical changes in the fluorescence of R601W were observed for 1-hexanol and *n*-hexyl-*β*-D-glucoside, point in the same direction.

The major change found for D611W is a strong quenching of fluorescence upon interaction with *n*-hexyl-*β*-D-glucoside. These data indicate that this area of loop 13 changes its position significantly with regard to neighboring areas of loop 13 but maintains its accessibility to acrylamide. The nearest neighbors responsible for major quenching could be the arginines at positions 601 and 602 or a methionine at position 618. Such a movement would require a high flexibility of this part of the molecule which is actually predicted by modeling, since this region is located in a random coil (*6*) between two helices (see also Figure 8).

E621W exhibits strong quenching and increased accessibility to acrylamide upon interaction with *n*-hexyl-*β*-D-glucoside. This probably also reflects the movement of the randomly coiled part of loop 13, although the specific interactions cannot be delineated currently with the data at hand. L630W exhibits the most prominent blue shift in the

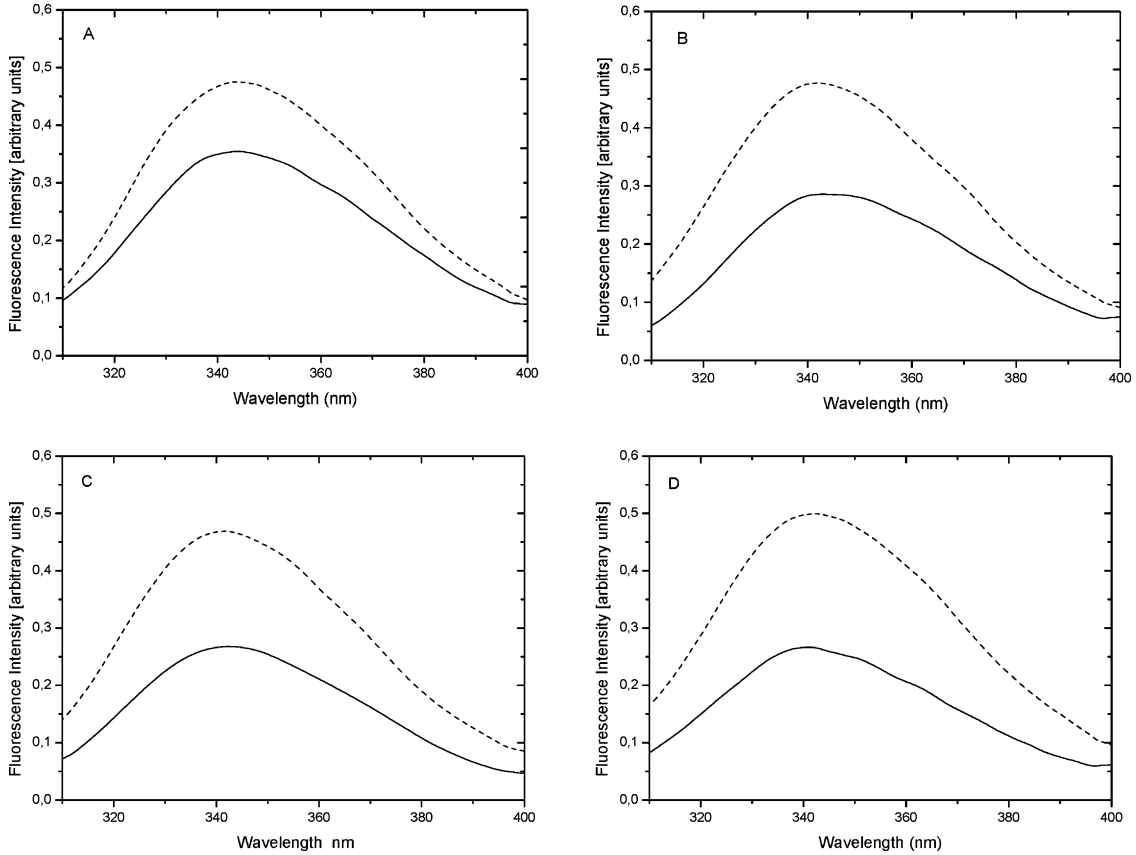

FIGURE 5: Effect of *n*-hexyl-*β*-D-glucoside on fluorescence emission spectra of single-Trp mutants of loop 13. The dotted lines show the corrected spectra in the absence of *n*-hexyl-*β*-D-glucoside, and the solid lines represent the effect of 100 *μ*M *n*-hexyl-*β*-D-glucoside on the intrinsic fluorescence. The peptide samples include R601W (A), D611W (B), E621W (C), and L630W (D).

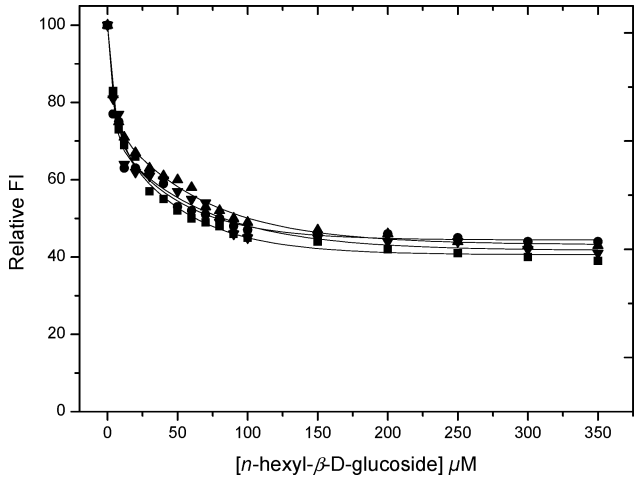

FIGURE 6: Titration of single-Trp mutants of loop 13 with *n*-hexyl-*β*-D-glucoside. All experiments were conducted as described in Experimental Procedures. Samples include R601W (■), D611W (●), E621W (▲), and L630W (▼). The percentage of quenching at a high *n*-hexyl-*β*-D-glucoside concentration was calculated from the data, and the values were fitted to a single-site binding equation using Prism (Graphpad, San Diego, CA) to calculate equilibrium dissociation constants. The K_d values for all mutants are summarized in Table 1.

Table 1: Acrylamide Accessibility and Apparent Affinity of *n*-Hexyl-*β*-D-glucoside to the Single-Trp Mutants of Truncated Loop 13[a]

peptide	*n*-hexyl-*β*-D-glucoside[b]	K_{SV}[c] (M^{-1})	K_d[d] (*μ*M)
R601W	−	21 ± 3	12 ± 4
	+	8 ± 1	
D611W	−	11 ± 2	8 ± 3
	+	8 ± 2	
E621W	−	12 ± 3	14 ± 6
	+	16 ± 2	
L630W	−	11 ± 1	9 ± 2
	+	8 ± 1	

[a] Parameters of *n*-hexyl-*β*-D-glucoside binding and acrylamide accessibility are derived from the data shown in Figures 6 and 7, respectively. [b] Quenching experiments were conducted in the presence (+) or absence (−) of 30 *μ*M *n*-hexyl-*β*-D-glucoside. [c] The Stern−Volmer quenching constants were determined from the slopes of the linear regression lines from plots of $F_0/F = 1 + K_{SV}$ [Q] (*14*). Values are means ± the standard deviation of two or three independent experiments. [d] The apparent equilibrium dissociation constants (K_d) were determined as described in Experimental Procedures. Values are means ± the standard deviation of two or three independent experiments.

fluorescence maximum and a strong quenching by *n*-hexyl-*β*-D-glucoside. Thus, major changes occur in this region of loop 13. A more condensed state of the molecule that positions Trp 630 close to the helical (hydrophobic) part between amino acids 599 and 607 could explain both effects. Experiments, however, which are currently under way must confirm this model by NMR and X-ray crystallography.

The proposed model can be compared to the schematic two-dimensional model presented recently for the interaction between phlorizin and loop 13 (*6*). There, phlorizin unfolds the segment of loop 13 between amino acid residues 608 and 620; *n*-hexyl-*β*-D-glucoside on the other hand appears to condense loop 13 and buries this segment between the two putative small helices. This assumption is supported by

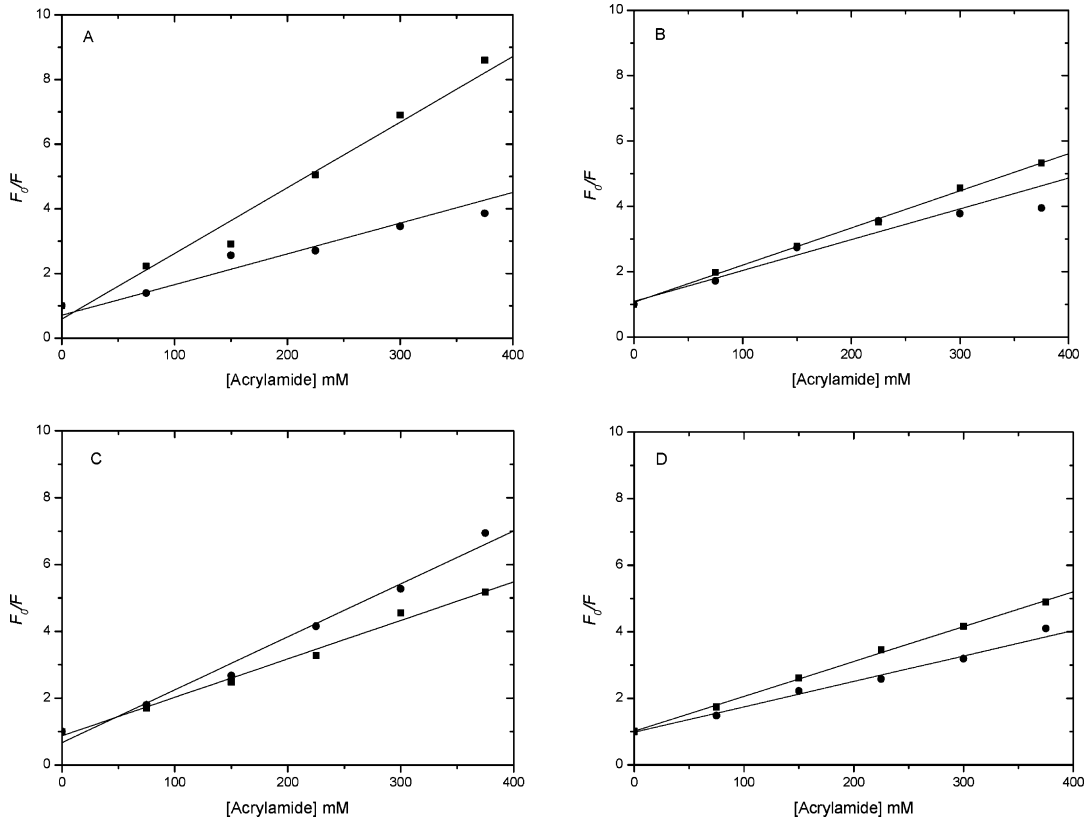

FIGURE 7: Stern−Volmer plots of Trp fluorescence quenching by acrylamide. Quenching experiments were conducted as described in Experimental Procedures. In each panel, the samples were investigated with (●) or without (■) 30 μM *n*-hexyl-β-D-glucoside. The peptide samples include R601W (A), D611W (B), E621W (C), and L630W (D). The slopes of the best fit linear regression lines for each data set (K_{SV} values) are shown in Table 1.

Table 2: Binding of Alkyl Glucoside Analogues to Mutant R601W[a]

glucoside	quenching[b] (%)		K_{SV}[c] (M^{-1})
n-octyl-β-D-glucoside	35	−	21 ± 3
		+	13 ± 3
n-octyl-α-D-glucoside	3	−	21 ± 3
		+	20 ± 2
trans-n-3-hexenyl-β-D-glucoside	20	−	21 ± 3
		+	14 ± 2
cis-n-3-hexenyl-β-D-glucoside	28	−	21 ± 3
		+	9 ± 2
n-hexyl-β-D-glucoside	26	−	21 ± 3
		+	8 ± 1
n-decyl-β-D-glucoside	16	−	21 ± 3
		+	18 ± 2

[a] The parameters are derived from the fluorescence quenching data and acrylamide accessibility (not shown). [b] Values represent fluorescence quenching in the presence of a concentration of each glucoside of 100 μM. [c] Quenching experiments were conducted in the presence (+) or absence (−) of each glucoside at a concentration of 30 μM.

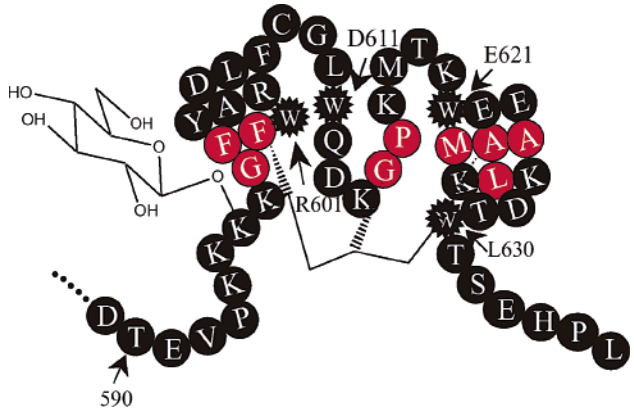

FIGURE 8: Schematic two-dimensional model of *n*-hexyl-β-D-glucoside binding to the part of truncated loop 13 of rabbit SGLT1. Red residues represent the assumed hydrophobic sites of interaction between the truncated loop 13 and *n*-hexyl-β-D-glucoside. Black stars represent single Trp mutations. C2 of the alkyl side chain is supposed to bind to the region between amino acids 598 and 601, C4 to amino acid residues 615 and 616, and C6 to the region between residues 621 and 630. For further information, see previous studies (*6*).

the observation that in additional fluorescence quenching studies *n*-hexyl-β-D-glucoside (data not shown) prevents phlorizin from interacting with loop 13.

Thus, irrespective of the model that is assumed, it is clear that *n*-hexyl-β-D-glucoside interacts with loop 13. Interestingly, this interaction is quite strong, and the apparent affinities are close to those observed for the inhibition of D-glucose transport by the intact SGLT1 in natural membranes (*18*). In addition, the relative potencies of the α- and β-glucosides and *cis* and *trans* derivatives of hexenyl glucosides on the transporter and in the isolated loop are comparable (*8*). These results support the view that loop 13 contains structural elements that mimic the conditions prevailing in the intact SGLT1.

However, a word of caution is also necessary. There is a discrepancy between the results obtained with the intact membrane-bound SGLT1 and this study with regard to the effect of chain length on binding. In this study, strong binding was observed for a chain length of six to eight carbons, whereas inhibition of D-glucose transport was maximal with

a chain length of 10 carbons in the alkyl side chain (*8*). This observation might suggest that in the intact SGLT1 other parts of the transporter also interact with alkyl glucosides. However, it is also possible that the conformation of the peptides used here and that of loop 13 in the intact carrier is different. The truncation of loop 13 removes the cysteine at position 560 which can form a disulfide bridge and thus alter the conformation *in vivo*. One additional site of interaction, most probably for the glucose part of alkyl glucoside, is the sugar binding site of the transporter, which is similar to the observation with phlorizin (*19*). This interaction predominates in the inhibition kinetics of the transport which is evident from the competition of D-glucose and *n*-hexyl-*β*-D-glucoside in the uptake studies.

ACKNOWLEDGMENT

Dedicated to Stefan Adamsmair on the occasion of his academic achievement. The careful secretarial work of Natascha Kist-Gruel and experimental help of Kirsten Michel are gratefully acknowledged.

Note added after ASAP posting. The Figure 1 legend contained an error in the version posted ASAP 8/7/04; the corrected version posted 8/11/04.

REFERENCES

1. Lin, J. T., Kormanec, J., Homerova, D., and Kinne, R. K. H. (1999) Probing Transmembrane Topology of the High-Affinity Sodium/Glucose Cotransporter (SGLT1) with Histidine-Tagged Mutants, *J. Membr. Biol. 170*, 243−252.
2. Hirayama, B. A., Loo, D. D., and Wright, E. M. (1997) Cation Effects on Protein Conformation and Transport in the Na^+/Glucose Cotransporter, *J. Biol. Chem. 272*, 2110−2115.
3. Loo, D. D., Hirayama, B. A., Gallardo, E. M., Lam, J. T., Turk, E., and Wright, E. M. (1998) Conformational changes couple Na^+ and glucose transport, *Proc. Natl. Acad. Sci. U.S.A. 95*, 7789−7794.
4. Hirayama, B. A., Diez-Sampedro, A., and Wright, E. M. (2001) Common mechanisms of inhibition for the Na^+/glucose (hSGLT1) and Na^+/Cl^-/GABA (hGAT1) cotransporters, *Br. J. Pharmacol. 134*, 484−495.
5. Diedrich, D. F. (1966) Competitive inhibition of intestinal glucose transport by phlorizin analogues, *Arch. Biochem. Biophys. 117*, 248−256.
6. Raja, M. M., Tyagi, N. K., and Kinne, R. K. H. (2003) Phlorizin Recognition in a C-terminal Fragment of SGLT1 Studied by Tryptophan Scanning and Affinity Labeling, *J. Biol. Chem. 278*, 49154−49163.
7. Xia, X., Lin, C. T., Wang, G., and Fang, W. (2004) Binding of phlorizin to the C-terminal loop 13 of the Na^+/glucose cotransporter does not depend on the [560−608] disulfide bond, *Arch. Biochem. Biophys. 425*, 58−64.
8. Kipp, H., Lin, J. T., and Kinne, R. K. H. (1996) Interactions of alkylglucosides with the renal sodium/D-glucose cotransporter, *Biochim. Biophys. Acta 1282*, 124−130.
9. Kipp, H., Kinne, R. K. H., and Lin, J. T. (1997) Synthesis of the photoaffinity label [1′-^{14}C]-6C-(azimethyl)octylglucoside and its reaction with isolated renal brush border membranes, *Anal. Biochem. 245*, 61−68.
10. Lin, J. T., Riedel, S., and Kinne, R. (1979) The use of octyl *β*-D-glucoside as detergent for hog kidney brush border membrane. *Biochim. Biophys. Acta 557*, 179−187.
11. Lowry, O. H., Rosebrough, N. J., Farr, A. L., and Randall, R. J. (1951) Protein measurement with the folin phenol reagent, *J. Biol. Chem. 193*, 265−275.
12. Gibbs, E. M., Hosang, M., Reber, B. F. X., Semenza, G., and Diedrich, D. F. (1982) 4-Azidophlorizin, a high affinity probe and photoaffinity label for the glucose transporter in brush border membranes, *Biochim. Biophys. Acta 688*, 547−556.
13. Lin, J. T., Hahn, K. D., and Kinne, R. K. H. (1982) Synthesis of phlorizin derivatives and their inhibitory effect on the renal sodium/D-glucose cotransport system, *Biochim. Biophys. Acta 693*, 379−388.
14. Lackowicz, J. R. (1999) *Principles of Fluorescence Spectroscopy*, Kluwer Academic/Plenum, New York.
15. Szmelcman, S., Schwartz, M., Silhavy, T. J., and Boos, W. (1976) Maltose transport in *Escherichia coli* K12. A comparison of transport kinetics in wild type and *λ*-resistant mutants as measured by fluorescence quenching, *Eur. J. Biochem. 65*, 13−19.
16. Zhao, H., and Kinnunen, K. J. (2002) Binding of the Antimicrobial Peptide Temporin L to Liposomes Assessed by Trp Fluorescence, *J. Biol. Chem. 277*, 25170−25177.
17. Breukink, E., Kraaij, C. V., Dalen, A. V., Demel, R. A., Siezen, R. J., Kruijff, B. D., and Kuipers, O. P. (1998) The Orientation of Nisin in Membranes, *Biochemistry 37*, 8153−8162.
18. Kipp, H., Kinne-Saffran, E. K., Bevan, C., and Kinne, R. K. H. (1997) Characteristics of renal Na^+-D-glucose cotransport in the skate (*Raja erinacea*) and shark (*Squalus acanthias*), *Am. J. Physiol. 273*, R134−R142.
19. Frasch, W., Frohnert, P. P., Bode, F., Baumann, K., and Kinne, R. (1970) Competitive inhibition of phlorizin binding by D-glucose and the influence of sodium: a study on isolated brush border membrane of rat kidney, *Pfluegers Arch. 320*, 265−284.
20. Church, R. F. R., Kende, A. S., and Weiss, M. J. (1965) Diazirines I. Some observations on the scope of the ammonia-hydroxylamin-*O*-sulfonic acid diaziridine synthesis. The preparation of certain steroid diaziridines and diazirines, *J. Am. Chem. Soc. 87*, 2665−2671.
21. Church, R. F. R., and Weiss, M. J. (1970) Diazirines II. Synthesis and properties of small functionalised diazirine molecules. Some observations on the reaction of a diaziridine with the iodine-iodine ion system, *J. Org. Chem. 35*, 2465−2471.

BI049106N